X-RAYS AND GAMMA-RAYS FROM ACCRETION FLOWS ONTO BLACK HOLES IN SEYFERTS AND X-RAY BINARIES

Andrzej A. Zdziarski

N. Copernicus Astronomical Center, Bartycka 18, 00-716 Warsaw, Poland

W. Neil Johnson

E. O. Hulburt Center for Space Research, Naval Research Lab, Washington, DC 20375, USA

Juri Poutanen

Uppsala Observatory, Box 515, S-75120 Uppsala, Sweden

Paweł Magdziarz and Marek Gierliński

Astronomical Observatory, Jagiellonian University, Orla 171, 30-244 Cracow, Poland

ABSTRACT

We review observations and theoretical models of X-ray/γ-ray spectra of radio-quiet Seyfert galaxies and of Galactic black-hole candidates (in the hard spectral state). The observed spectra share all their basic components: an underlying power law, a Compton-reflection component with an Fe Kα line, low-energy absorption by intervening cold matter, and a high-energy cutoff above $\sim$ 200 keV. The X-ray energy spectral index, α, is typically in the range ~ 0.8–1 in Seyfert spectra from *Ginga*, *EXOSAT* and OSSE. The hard-state spectra of black-hole candidates Cyg X-1 and GX 339-4 from simultaneous *Ginga*/OSSE observations have $\alpha \simeq 0.6$–0.8. The Compton-reflection component corresponds to cold matter (e.g., inner or outer parts of an accretion disk) covering a solid angle of $\sim (0.4$–$1) \times 2\pi$ as seen from the X-ray source. The spectra are cut off in soft γ-rays above $\sim$ 200 keV. The broad-band spectra of both Seyferts and black-hole sources are well fitted by Compton upscattering of soft photons in thermal plasmas. Our fits yield the thermal plasma temperature of $\sim$ 100 keV and the Thomson optical depth of $\tau \sim 1$. A fraction of the luminosity emitted nonthermally appears to be small and it can be constrained to $\lesssim 15\%$ in the Seyfert galaxy NGC 4151. The spectra are cut off before 511 keV, which is strongly suggestive of a thermostatic role of $e^{\pm}$ pair production in constraining the temperature and optical depth of the sources. The source geometry is compatible with a patchy corona above a cold disk in Seyferts, but not in Cyg X-1. In the latter, the relative weakness of reflection is compatible with reflection of emission of a hot inner disk from outer disk regions.

Keywords: galaxies: nuclei – galaxies: Seyfert – X-rays: galaxies – gamma-rays: observations – radiation mechanisms: thermal – stars: individual: (Cyg X-1, GX 339-4)

1. INTRODUCTION

Seyfert galaxies are the first class of objects in which we are able to directly probe the gravitational potential near a black hole. This has been achieved thanks to the discovery by the *ASCA* observatory (Tanaka, Inoue & Holt 1994) of broad Fe Kα lines from several Seyfert 1s (Tanaka et al. 1995; Fabian et al. 1995; Iwasawa et al. 1996). The width of the lines, $\sim c/3$ or more, requires the lines originate in large part at radial distances of $6GM/c^2$ or even less (Iwasawa et al. 1996). The peak energies of the narrow cores of the lines are close to 6.4 keV, which shows the lines are emitted by cold and dense media, with Fe being at most mildly ionized.

The lines originate when X-rays irradiate cold matter. Photons with energies above the Fe K edge, $\gtrsim 7$ keV, are able to ionize the K shell of an Fe atom or ion. Since the L shell is occupied (unless for He-like and H-like Fe ions), the ion becomes excited. The deexcitation proceeds in most cases through an L-to-K transition. The transition energy, ≥ 6.4 keV, goes into either an ejection of an outer shell (Auger) electron, or into emission of a Kα photon. The probability of the latter process is about 50% (e.g., George & Fabian 1991). The resulting fluorescent Kα line is broadened by the Doppler effect and gravitationally.

A very important process associated with the fluorescent formation of Fe Kα lines is Compton reflection (White, Lightman & Zdziarski 1988; Lightman & White 1988). In this process, X-rays and γ-rays (hereafter Xγ) irradiating the cold matter get Compton-scattered (in one or more scattering events) back to the observer. Compton reflection of a power-law spectrum typical for Seyferts forms a characteristic continuum peaked (in νF_ν) around 30 keV. Below the peak, bound-free absorption becomes important and incident photons are likely to get absorbed. The bound-free cross section of cosmic-composition matter increases (except at ionizatoin

edge energies) with decreasing energy, and it becomes larger than the Thomson cross section below $\sim$ 10 keV. Above the peak, Klein-Nishina effects become important. Namely, a photon loses a substantial part of its energy in a scattering, which occurs preferentially forward, and its cross section decreases with energy. These effect results in a steep cutoff of the reflected spectrum above $\sim$ 100 keV. The presence of a Compton-reflected spectral component has been discovered in the spectra of Seyferts by *Ginga* (Pounds et al. 1990; Nandra & Pounds 1994). The relative normalization of the reflected component with respect to the direct one in the spectra of Seyfert 1s corresponds to the solid angle of the reflector close to 2π (Nandra & Pounds 1994; Zdziarski et al. 1995; Gondek et al. 1996). This strongly suggests that the reflector is a cold accretion disk. This conclusion is further supported by the fits to the Kα line profiles by emission of relativistic disks (extending to the minimum stable orbit, e.g., Tanaka et al. 1995) and the large equivalent widths of the Kα lines, EW$\sim$ 200 eV on average (Nandra et al. 1996).

Thus, the results of *ASCA* and *Ginga* lead to a picture with the Xγ emission in Seyfert 1s typically taking place above the surface of an accretion disk. As discussed above, we understand relatively well the reflected, secondary, component of the emission. On the other hand, the origin of the incident, *primary*, radiation is much less understood. In order to understand its origin, we need to study broad-band, Xγ spectra of Seyferts. In X-rays, the intrinsic spectra turn out to be simple power laws (see §2 below), which only weakly constrain their origin. A key observable needed to understand the origin of the primary spectra is the spectral shape at high energies, in particular any spectral break or cutoff, or a spectral feature. This key information can be provided by soft γ-ray observations by OSSE (Johnson et al. 1993) aboard *Compton Gamma Ray Observatory*, as well as future soft γ-ray experiments, e.g., *INTEGRAL* (Winkler 1994). In this work, we review the available Xγ spectra from Seyferts and discuss resulting constraints on physical processes in the radiation sources (see also reviews by Svensson 1996; Zdziarski et al. 1996).

We also discuss the spectral properties of Galactic black-hole candidates in the hard (so-called 'low') state (see Nowak 1995). We consider spectra of GX 339-4 and Cyg X-1. The spectra are very similar to those of Seyferts and consist of an underlying power-law, a Compton reflection component, and a high-energy cutoff at $\sim$ 200 keV. This remarkable similarity between Seyfert and stellar-mass black-hole sources appears to reflect the shared origin of the emission from an accretion flow onto a black hole. We find that the intrinsic power laws with the cutoff in both classes of objects are well modeled by thermal Compton upscattering in mildly relativistic plasmas of moderate Thomson optical thickness ($kT \sim 100$ keV, $\tau \sim 1$).

2. SPECTRA OF IC 4329A AND OF AVERAGE SEYFERT SAMPLES

As yet, relatively few broad-band, Xγ spectra of Seyferts are available. Those include the spectrum

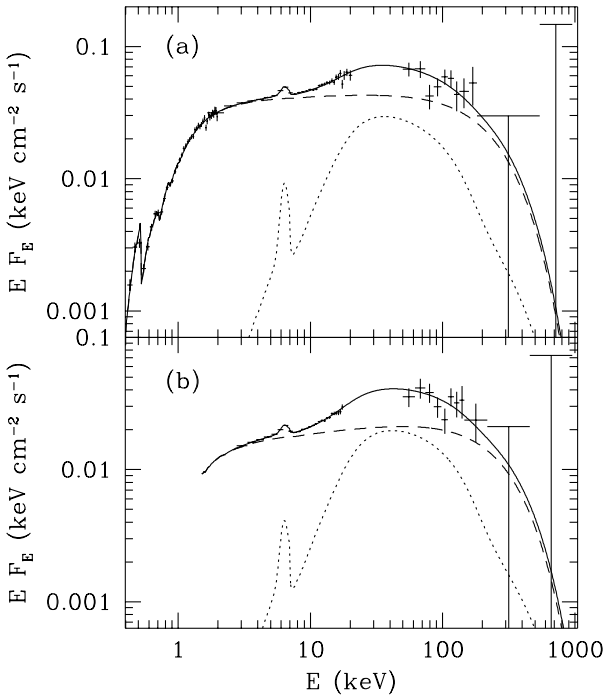

Figure 1: The broad-band Xγ spectra of Seyfert 1s. *(a)* The *ROSAT*/*Ginga*/OSSE spectrum of IC 4329A. *(b)* The average spectrum (*crosses*) of 5 radio-quiet Seyfert 1s detected by both OSSE and *Ginga*. The upper limits here and in figures below are 2-σ. The dashed curves represent the best-fit thermal Comptonization spectra of PS96. The dotted curves represent the absorbed reflected component including the fluorescent Fe Kα line. The solid curves give the sum.

of IC 4329A (a Seyfert 1) from *ROSAT*, *Ginga*, and OSSE (Madejski et al. 1995). The spectrum (fitted as in Zdziarski et al. 1996) is shown in Figure 1a. It consists of an underlying power law with the energy spectral index of $\alpha = 0.94 \pm 0.03$ and a reflection component corresponding to the solid angle of $\Omega/2\pi = 0.74^{+0.17}_{-0.16}$ (assuming the viewing anle of 30° in angle-dependent reflection Green's functions of Magdziarz & Zdziarski 1995 and using the elemental abundances of Anders & Grevesse 1989). There is a cutoff in the spectrum above $\sim$ 200 keV; when the spectrum is fitted with an e-folded power law, the e-folding energy is $E_c = 0.3^{+0.2}_{-0.1}$ MeV. (We use XSPEC, see Arnaud 1996, for spectral fitting, and the quoted errors are for 90% confidence limit based on a $\Delta\chi^2 = 2.7$ criterion.)

A similar cutoff above $\sim$ 200 keV is seen in the average spectrum of 5 radio-quiet Seyfert 1s observed 25 times by *Ginga* and 14 times by OSSE (Gondek et al. 1996), shown in Figure 1b. The parameters of the fit with an e-folded power law are $\alpha = 0.90 \pm 0.05$, $\Omega/2\pi = 0.76 \pm 0.15$, and $E_c = 0.7^{+2.0}_{-0.3}$ MeV (assuming the abundances of Anders & Ebihara 1982). A very similar average spectrum is also obtained for 7 radio-quiet Seyfert 1s observed 41 times by *EXOSAT* and 18 times by OSSE (Gondek et al. 1996).

A major question for our understanding of the AGN

phenomenon is the origin of the underlying cut-off power law spectrum. Models with synchrotron emission predict simultaneous IR/X-ray variability, which is not observed. Also, the cutoff above 200 keV would then require a fine-tuned sharp cutoff in the distribution of the emitting relativistic electrons. The most likely physical process responsible for the underlying spectra appears to be Compton scattering in a thermal plasma. The formation of power-law spectra in this model is due to superposition of relatively narrow scattering profiles from subsequent orders of scattering (e.g., Svensson 1996). The spectral index is a function of the optical depth and temperature of the plasma, and there is high-energy cutoff in the spectrum at energies above a few times kT. The plasma in Seyfert 1s is *not* optically thick (Zdziarski et al. 1994), which precludes the use of formulae of Sunyaev & Titarchuk (1980). Until recently, there have been no ready-to-use, accurate, formulae for spectra of $\tau \lesssim 1$ plasmas (as discussed in Poutanen & Svensson 1996, hereafter PS96). Instead, power-laws with exponential cutoffs have been commonly used (see above).

Here, we use the code of PS96 for thermal Comptonization in active regions above the surface of a disk. The active regions are assumed to have the form of hemispheres (with the radial optical depth equal τ) on the disk surface. The code gives highly accurate results, which agree with those obtained with a Monte Carlo method (Stern et al. 1995; PS96). Here, we use this code to fit IC 4329A (see also Poutanen, Svensson & Stern 1997) and the average *Ginga*/OSSE spectrum of Seyfert 1s (Gondek et al. 1996). Our preliminary fits give $\tau = 1.3^{+0.4}_{-0.2}$, $kT = 100^{+10}_{-30}$ keV, and $\tau = 1.0^{+0.4}_{-0.2}$ and $kT = 130^{+30}_{-40}$ keV, respectively. The model spectra are shown by the curves in Figures 1a, b.

The statistics of the OSSE data of the two above spectra is relatively limited, and thus the cutoff is not very well constrained. Therefore, we also consider the co-added spectrum of all Seyfert 1s (except NGC 4151) detected by OSSE through 1995 (McNaron-Brown et al. 1997). The sample consists of 29 observations of 12 Seyfert 1s. NGC 4151, whose flux in the OSSE range is an order of magnitude higher than that of other Seyfert 1s, is excluded in order to avoid the dominance of the spectrum by a single object. That spectrum, shown in Figure 2a, has the shape indistinguishable from that of the co-added OSSE spectra of Gondek et al. (1996). By this we hereafter mean that the two spectra can be fitted with the same model with $\Delta\chi^2 < 2.7$ with respect to the sum of χ^2 for the two individual fits. The present OSSE spectrum shows a clear high-energy cutoff above ~ 150 keV. However, the OSSE spectrum starts at 50 keV only and it does not allow to determine the X- ray spectral index and the normalization of the reflection component, which quantities are both are important for determining the plasma temperature. Therefore, while fitting the average OSSE spectrum we constrain the X-ray spectrum at the best-fit values obtained for the *Ginga*/OSSE average spectrum ($\alpha = 0.90 \pm 0.05$, $\Omega/2\pi = 0.76 \pm 0.15$). Our preliminary fit results are again very similar to those above, $\tau = 1.2^{+0.4}_{-0.3}$ and $kT = 110^{+40}_{-30}$ (shown by the curves in Figure 2a).

We compare now the average OSSE spectrum of

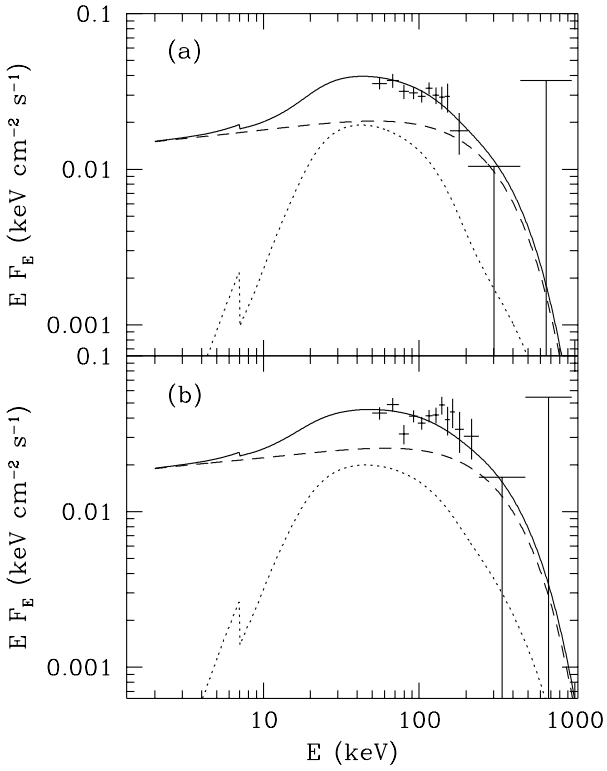

Figure 2: The average spectra (*crosses*) of radio-quiet Seyferts detected by OSSE (McNaron-Brown et al. 1997). The dashed curves represent the best-fit thermal Comptonization spectra of PS96 (without showing absorption at soft X-rays). The dotted curves represent the reflected component. The solid curves give the sum. *(a)* The Seyfert 1 sample (excluding NGC 4151). *(b)* The Seyfert 2 sample.

Seyfert 1s with that of Seyfert 2s detected by OSSE (8 objects observed 19 times through 1995; McNaron-Brown et al. 1997). We find that the spectrum, shown in Figure 2b, is statistically indistinguishable from that of Seyfert 1s above, and it again shows a cutoff above ~ 200 keV. When we fit it with the best-fit constraints at X-rays as obtained by Gondek et al. (1996) for Seyfert 1s (except that the disk viewing angle, important for reflection, is fixed at 60°, compatible with the AGN unified model, Antonucci 1993), we obtain $\tau = 1.1^{+0.2}_{-0.2}$ and $kT = 110^{+20}_{-20}$ (corresponding to the curves in Figure 2b). The fact that these fits give results virtually identical to those of Seyfert 1s strongly supports the unified AGN model, according to which Seyfert 1s and 2s differ only by orientation with respect to the observer (Antonucci & Miller 1985; Antonucci 1993). It also shows that the characteristic column densities of the obscuring torii in the considered sample are such that photons at 50 keV are not strongly absorbed, which corresponds to $N_{\rm H} \lesssim 10^{24}$ cm^{-2}.

The plasma inferred here to exist in Seyferts has $\tau \sim 1$ and $kT \sim 100$ keV, i.e., it has larger optical depth and lower temperature from the parameters considered before, e.g., by Zdziarski et al. (1994) and Stern et al. (1995). The former authors fitted the spectrum of IC 4329A by an e-folded power law with reflection, and only then found the plasma parameters corresponding to the best fit. However, the actual shape of the high-energy cutoff from thermal Comptonization is not described by an e-folded power law, and thus that procedure led to an underestimate of τ and an overestimate of kT. On the other hand, Stern et al. (1995) considered models with hot, pure $e^{\pm}$-pair, plasma regions attached to the disk surface and compared the results with the distribution of X-ray spectral indices in Seyfert 1s of Nandra & Pounds (1994). This implied that $\tau \lesssim 0.3$ correspond to hot plasmas in Seyferts. This disagrees with the present fits, which implies that some of the assumption of Stern et al. are not satisfied. It can be either that the active regions are located at some height *above* the disk surface (Svensson 1996), or the plasma is not pure $e^{\pm}$ pairs, or both.

3. NGC 4151 AND LIMIT ON NONTHERMAL PROCESSES

As mentioned above, the brightest radio-quiet Seyfert is NGC 4151, observed by OSSE 10 times during 1991-96 (Johnson et al. 1997). Its X-ray spectrum is strongly absorbed by $N_{\rm H} \sim 10^{23}$ cm^{-2}. Therefore, it is difficult to determine the form of the intrinsic X-ray spectrum. Xγ observations before 1991 show hard intrinsic X-ray spectra, with $\alpha \sim 0.3$–0.8 and no detectable Compton-reflection component (e.g. Yaqoob et al. 1993). On the other hand, contemporaneous Xγ observations in 1991–93 June show the object in a soft state, with $\alpha \sim 0.80 \pm 0.05$ (when fitted with thermal Comptonization, Zdziarski, Johnson & Magdziarz 1996, hereafter ZJM96). This X-ray spectral index is within the 1-σ range of those observed on average in Seyfert 1s, $\langle\alpha\rangle = 0.95$, $\sigma = 0.15$ (Nandra & Pounds 1994). Furthermore, the *Ginga*/OSSE observation of 1991 June/July shows the presence of a Compton-reflection component with $R \simeq 0.4 \pm 0.2$,

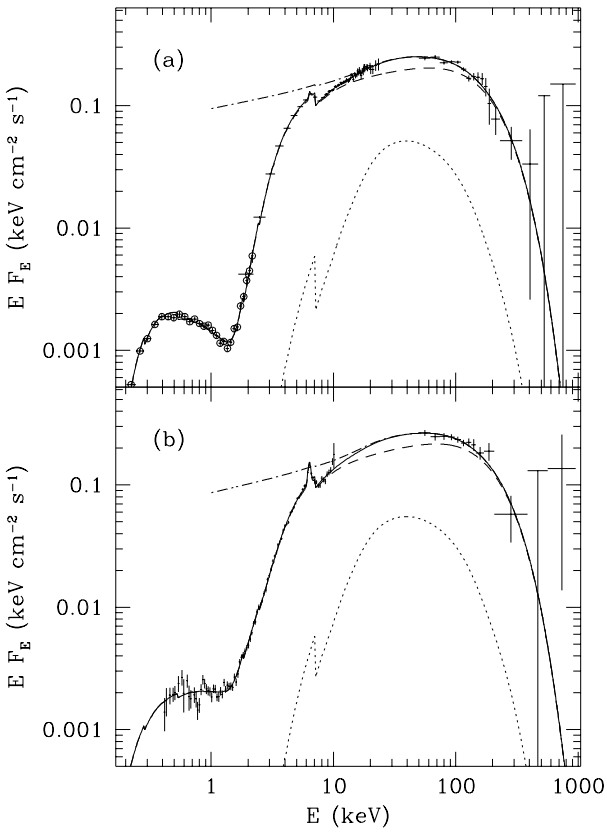

Figure 3: The Xγ spectra of NGC 4151 observed by *(a) ROSAT*, *Ginga* and OSSE in 1991 June/July and *(b)* by *ASCA*and OSSE in 1993 May (ZJM96). The dot-dashed curves show the unabsorbed spectrum (without the Fe Kα line and the separate soft X-ray component, dominant below 1 keV). The dashed curves represent the best-fit thermal Comptonization spectra of ZJM96. The dotted curves represent the absorbed reflected component. The solid curves give the total model spectra.

see Figure 3a (ZJM96). Also, the OSSE spectra of NGC 4151 are statistically not distinguishable from the average OSSE spectrum of Seyfert 1s (ZJM96). The corresponding plasma parameters determined by ZJM96 are $\tau \sim 1.3$, $kT \sim 60$ keV. Thus, the only characteristic distinguishing the soft state of NGC 4151 from other Seyfert 1s appears to be a large absorbing column.

The simultaneous *ASCA*/OSSE spectrum of 1993 May (ZJM96) does not allow a determination of the strength of Compton reflection, which leads to some ambiguity in determining the intrinsic spectrum. If the same amount of reflection as for the *Ginga*/OSSE observation is assumed, the intrinsic spectrum is the same within statistical uncertainties as the *Ginga*/OSSE spectrum, see Figure 3b (ZJM96).

OSSE observations of NGC 4151 yield spectra relatively constant in shape, and with the normalization varying within a factor of ~ 2 (ZJM96; Johnson et al. 1997). Thus, the co-added spectrum is representative of time-resolved spectra but it gives much

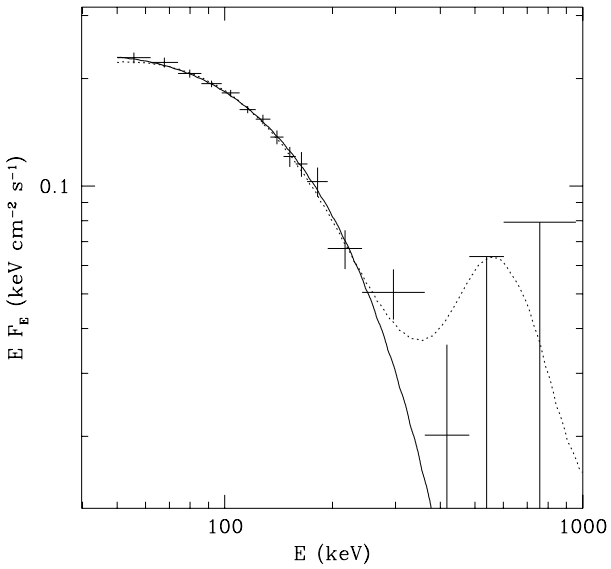

Figure 4: The average OSSE spectrum of NGC 4151 (Johnson et al. 1997). The solid curve gives the best-fit thermal Comptonization model. The dashed curve corresponds to the spectrum with the strongest allowed fraction, 17%, of nonthermal processes in the source. See text.

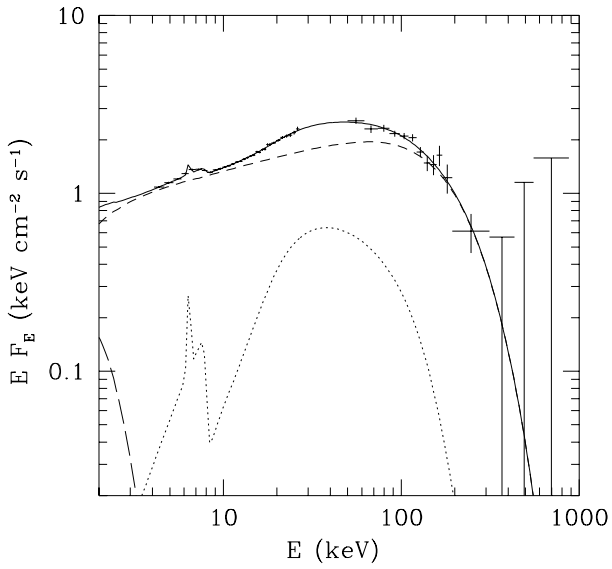

Figure 5: An Xγ spectrum of GX 339-4 observed simultaneously by *Ginga* and OSSE and fitted by the thermal Comptonization model of ZJM96 (dashed curve) and Compton reflection (dotted curve). The long dashes correspond to a soft component due to blackbody disk emission. The solid curve gives the sum.

better statistics at high energies. The spectrum is shown in Figure 4. We again obtain that the average NGC 4151 spectrum is statistically not distinguishable from that of the average Seyfert-1 spectrum. This again argues for NGC 4151 being a relatively average Seyfert 1 rather than a peculiar object. The plasma parameters for the average spectrum of NGC 4151 fitted with the thermal Comptonization model of ZJM96, $\tau \sim 1.3$, $kT \sim 70$ keV, are similar to those in other Seyfert 1s.

We see in Figure 4 that the average OSSE spectrum of NGC 4151 shows a cutoff well-fitted by the thermal Comptonization model. We can use this spectrum to constrain the presence of nonthermal processes in the Xγ source in NGC 4151. We consider a model in which a fraction of the available power is used to accelerate selected electrons (or $e^{\pm}$ pairs) to relativistic energies, and the rest is distributed approximately equally among the remaining electrons, i.e., it heats the plasma. Such a model for NGC 4151 was proposed by Zdziarski, Lightman & Maciołek-Niedźwiecki (1993). The presence of nonthermal acceleration gives rise to a tail on top of the thermal spectrum. This tail is due to both Compton scattering by the relativistic electrons as well as due to annihilation of $e^{\pm}$ pairs from the resulting pair cascade (see Svensson 1987; Lightman & Zdziarski 1987). We repeat the calculations of Zdziarski et al. (1993) for the average OSSE spectrum of NGC 4151 (Johnson et al. 1997). We find that the presence of a nonthermal tail does not improve the fit to the spectrum. The 90% confidence limit on the nonthermal fraction is 0.17. The spectrum corresponding to this limit is shown in Figure 4 in dotted line.

4. GALACTIC BLACK-HOLE CANDIDATES IN THE HARD STATE

It is very intriguing that some Galactic black-hole candidates observed in the hard (so-called 'low') state have high-energy spectra virtually identical to those of Seyfert 1s. One example is the hard-state spectrum of GX 339-4 observed simultaneously by *Ginga* and OSSE in 1991 September (Ueda et al. 1994; Grabelsky et al. 1995). The spectrum, re-analyzed and fitted with the thermal Comptonization model of ZJM96, is shown in Figure 5. The spectral parameters are virtually identical to those of NGC 4151, with $kT \simeq 70$ keV, $\alpha = 0.8$ (corresponding to $\tau \sim 1.2$), and a Compton reflection component corresponding to $\Omega/2\pi \simeq 0.5$.

The archetypical black-hole candidate Cyg X-1 was observed four times by *Ginga* and OSSE simultaneously in 1991 June (Gierliński et al. 1996; 1997). The spectra correspond to the hard ('low') state of this source. They show $\alpha \simeq 0.6$, a reflection component, and a high-energy cutoff above ~ 150 keV similar to that of AGNs. However, that cutoff is sharper than one possible to obtain with a uniform thermal plasma. Gierliński et al. (1997) fitted that spectrum with the sum of Comptonization spectra in two plasma clouds with $\tau \sim 1$, $kT \simeq 140$ keV and $\tau \simeq 7$ and $kT \simeq 50$ keV, respectively. The first component has the parameters very similar to those obtained above for Seyeferts. It may well be that high-energy cutoffs in Seyferts are also complex, but the limited statistics of Seyfert spectra precludes constraining fits more complex than those corresponding to uniform plasma in the vicinity of cold matter. The similarity between the Xγ spectra of Seyferts

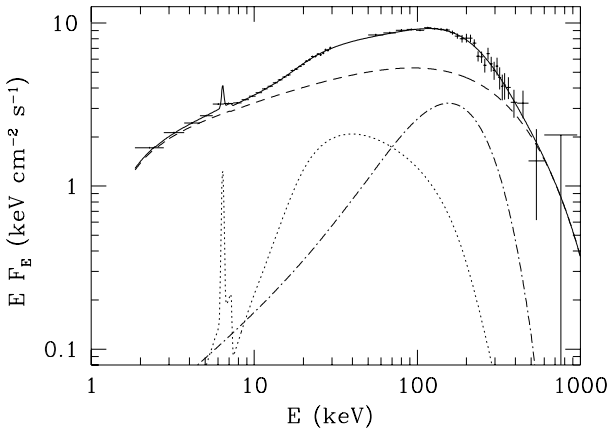

Figure 6: An Xγ spectrum of Cyg X-1 observed simultaneously by *Ginga* and OSSE and fitted by the sum of a power law with an exponential cutoff (dashed curve), Compton reflection (dotted curve), and an additional thermal-Compton component from an optically thick plasma (dot-dashed curve). The solid curve gives the sum. From Gierliński et al. (1997).

and Galactic black hole sources is, in fact, expected due to scale-free character of both disk accretion and two-body processes.

5. GEOMETRY

We can constrain the geometry of thermal Comptonization sources by considering energy balance. There are two main conditions. First, a cloud of hot plasma will upscatter incident soft, seed, photons into the Xγ range, in which process the incident soft photon flux will get amplified by an amplification factor, A, dependent on τ and kT. This can be determined by spectral fitting, and for sources with hard spectra (with $\alpha < 1$), $A \gg 1$. Thus,

$$L_{\rm X\gamma} = A(\tau, kT) L_{\rm soft}^{\rm incident}.$$

Second, the Xγ flux irradiating cold matter will get reprocessed and reradiated mostly as soft photons (the integrated albedo for Compton reflection is small, $a \sim 0.1$, e.g., Magdziarz & Zdziarski 1995). For an isotropic Xγ source,

$$L_{\rm soft}^{\rm reprocessed} = (\Omega/2\pi)(1-a) L_{\rm X\gamma},$$

(where Ω is the solid angle subtended by the reflecting and reprocessing medium, as in Sections above). From observations, $\Omega \sim 2\pi$ (see above). Thus, $L_{\rm soft}^{\rm reprocessed} \gg L_{\rm soft}^{\rm incident}$ when $A \gg 1$. This rules out a homogeneous corona geometry (proposed by Haardt & Maraschi 1993) for objects with hard spectra ($\alpha \lesssim 1$).

Note that the above result is different from that of Haardt, Maraschi & Ghisellini (1994), who pointed out that $L_{\rm UV} \gg L_{\rm X\gamma}$ often observed in Seyferts (Walter & Fink 1993) also rules out the dissipative, homogeneous, corona model, in which the two quantities are predicted to be similar. These observations require that dissipation takes place in the cold matter (presumably an accretion disk), not only in the corona (as assumed in Haardt & Maraschi 1993).

A geometry that can solve both of the problems above is a *patchy* corona, in which the hot plasma forms small active regions above the disk surface. The ratio of the size of an active region to its average height above the disk determines what fraction of the reprocessed photons (with $L_{\rm soft}^{\rm reprocessed}$) returns to the active region, and thus becomes $L_{\rm soft}^{\rm incident}$ (Stern et al. 1995; Svensson 1996). For the characteristic parameters of compact objects found here ($\tau \sim 1$ and $kT \sim 100$ keV), active regions located above the disk surface at a height similar to the size of the active region satisfy the energy balance (Fig. 2 in Svensson 1996). On the other hand, the UV luminosities in Seyferts are often much larger than the Xγ ones, which requires that the active regions cover a relatively small fraction of the disk surface. That fraction is determined by both the luminosity ratio and the ratio of the dissipation rate in the corona to that in the disk (Haardt et al. 1994).

Thus, patchy coronae provide a good model for sources with $\Omega \sim 2\pi$ (as determined by the Compton reflection fits). The reflecting (and reprocessing) disks and their patchy coronae in Seyferts often extend to the minimum stable orbit, as indicated by the observations of broad Fe Kα lines by *ASCA* (e.g., Fabian et al. 1995). If $\Omega \ll 2\pi$ (as seems to be the case in Cyg X-1, see above), the hot sources cannot be located above a disk. A possible geometry is then a hot inner disk and a cold outer disk (as discussed for Cyg X-1 by Gierliński et al. 1997). This is also compatible with the narrowness of the Fe Kα line in Cyg X-1 (Ebisawa et al. 1996).

6. ELECTRON-POSITRON PAIRS

The next issue we consider is the presence of $e^{\pm}$ pairs in the sources. The role of pair production is qualitatively different in sources with and without nonthermal processes. When nonthermal processes dominate, Compton upscattering of seed soft photons by nonthermal, relativistic, electrons can easily produce photons well above the threshold for $e^{\pm}$ pair production, 511 keV. The photons with energies > 511 keV can be absorbed in photon-photon interactions, which leads to a prediction of a cutoff in the spectrum above 511 keV. The produced pairs can be relativistic as well and further Compton upscatter the seed photons to energies above 511 keV, which gives rise to a pair cascade (Svensson 1987; Lightman & Zdziarski 1987). The pairs annihilate, however, only after loosing most of their energy and having joint the low-energy, thermal, electron distribution. Therefore, the annihilating pairs have typically energies much lower than the energies of electrons that lead to the pair production process. Thus, a common prediction of nonthermal models is the presence of a strong and $e^{\pm}$ pair annihilation feature around 511 keV (e.g., Svensson 1987; Lightman & Zdziarski 1987). Such features have not been observed in AGNs. The average OSSE spectrum of NGC 4151 constrains the power channeled into nonthermal processes (which could lead to a pair annihilation feature, see Figure 4), to less than

17% (Section 3). Also, no annihilation feature is seen in the spectra of the Galactic black-hole source Cyg X-1 (Phlips et al. 1996). Therefore, acceleration of electrons to relativistic energies appears to play at most a minor role in black hole accretion flows.

On the other hand, good fits to the spectra of compacts objects are obtained with thermal models (see Sections 2-4). In thermal sources, pairs and electrons have a Maxwellian distribution. Compton scattering of seed photons by the pairs and electrons determines the Xγ spectrum, which may extend above 511 keV. The pair production rate follows then from the shape of the spectrum. The pair annihilation rate depends mostly on the optical depth of the source. In pair equilibrium, the two quantities are equal, which condition determines the compactness parameter,

$$\ell \equiv l\sigma_{\rm T}/rm_e c^3$$

(where l and r are the luminosity and size, respectively, of an active region, and $\sigma_{\rm T}$ is the Thomson cross section), at which the source is made entirely of pairs in steady state (Svensson 1984). This represents the upper limit to the actual compactness, which can be is lower if there are some ionization electrons in addition to $e^{\pm}$ pairs. The compactness requires for pair-domination is also lower if some fraction of the luminosity is channeled into nonthermal processes (e.g., ZJM96). The plasma parameters inferred for most of the sources considered in this review are $\tau \sim 1$ and $kT \sim 100$ keV, for which the maximum $\ell \simeq 300$ (see Fig. 3 in Svensson 1996). Such a compactness is possible for sources accreting at a fraction of the Eddington limit.

Note that even if a thermal source is made entirely of $e^{\pm}$ pairs, no distinct pair annihilation feature around 511 keV is visible in the spectrum (Maciołek-Niedźwiecki, Zdziarski & Coppi 1995). Thus, the lack of detection of annihilation lines in the spectra of compact objects is still compatible with their composition of thermal $e^{\pm}$ pairs.

The way pair production constrains source parameters in thermal sources is *not* by pair absorption (important above 511 keV in nonthermal sources). Rather, pair production leads to an increase of the number of particles in the source. If the total power supplied to the particles is fixed, this leads to a decrease of the average energy per particle, or the temperature. The lowered temperature leads to fewer photons upscattered above 511 keV, which in turn lowers the pair production rate. The fact that the Xγ spectra of compact objects are cut off close to 511 keV (at ~ 200 keV, see above), strongly suggests that this pair thermostat operates in Seyferts and black-hole binaries. The typical plasma temperature of 100 keV found here is such that the sources are just at the onset of copious pair production.

7. CONCLUSIONS

Our main new result is that the plasma parameters in Seyferts and in Galactic black-hole candidates in the hard state are $\tau \sim 1$ and $kT \sim 100$ keV. This has been obtained by direct fitting the available Xγ spectra with thermal Comptonization models. The spectra are cut off at energies below the electron rest energy, which indicates that $e^{\pm}$ pair production is an important process. Nonthermal processes appear to play at most a minor role.

The presence of Compton-reflection components shows that there is cold matter subtending a substantial solid angle as seen from the Xγ source. In Seyferts, a patchy corona above a cold accretion disk is consistent with the data. On the other hand, this geometry is not compatible with the spectrum of Cyg X-1, in which the cold matter subtends a relatively small solid angle, consistent with reflection from an outer disk. This is also consistent the lack of detection of broad Fe Kα lines in black-hole sources, which argues against the presence of cold matter close to the innermost stable orbit.

ACKNOWLEDGMENTS

This research has been supported in part by NASA grants and contracts and the Polish KBN grants 2P03D01008, 2P03D01410, 2P03C00511p01, and 2P03C0511p4. We thank Bronek Rudak for help with fitting GX 339-4.

REFERENCES

Anders E., Ebihara M., 1982, Geochim. Cosmochim. Acta 46, 2363

Anders E., Grevesse N., 1989, Geochim. Cosmochim. Acta 53, 197

Antonucci R. R. J., 1993, ARAA, 31, 473

Antonucci R. R. J., Miller J. S., 1985, ApJ, 297, 621

Arnaud K. A., 1996, in: Jacoby G. H., Barnes J. (eds.) Astronomical Data Analysis Software and Systems V. ASP Conf. Series Vol. 101, San Francisco, p. 17

Ebisawa, K., Ueda Y., Inoue H., Tanaka Y., White N. E., 1996, ApJ, 467, 419

Fabian A. C., Nandra K., Reynolds C. S., Brandt W. N., Otani C., Tanaka Y., Inoue H., Iwasawa K., 1995, MNRAS, 277, L11

George I. M., Fabian A. C., 1991, MNRAS, 249, 352

Gierliński M., Zdziarski A. A., Johnson W. N., et al., 1996, in: Zimmermann H. U., Trümper J., Yorke H. (eds.) MPE Report 263, Röntgenstrahlung from the Universe, p. 139

Gierliński M., Zdziarski A. A, Done C., Johnson W. N., Ebisawa K., Ueda Y., Haardt F., Phlips B. F., 1997, MNRAS, submitted

Gondek D., Zdziarski A. A., Johnson W. N., George I. M., McNaron-Brown K., Magdziarz P., Smith D., Gruber D. E., 1996, MNRAS, 282, 646

Grabelsky D. A., Matz S. M., Purcell W. R., et al., 1995, ApJ, 441, 800

Haardt F., Maraschi L., 1993, ApJ, 413, 507

Haardt F., Maraschi L., Ghisellini G., 1994, ApJ, 432, L95

Iwasawa K., et al., 1996, MNRAS, 282, 1038

Johnson W. N., et al., 1993, ApJS, 86, 693

Johnson W. N., McNaron-Brown K., Kurfess J. D., Zdziarski A. A., Magdziarz P., Gehrels N., Reichert G. A., 1997, ApJ, submitted

Lightman A. P., White T. R., 1988, ApJ, 335, 57

Lightman A. P., Zdziarski A. A., 1987, ApJ, 319, 643

Maciołek-Niedźwiecki A., Zdziarski A. A., Coppi P. S., 1995, MNRAS, 276, 273

Madejski G. M., Zdziarski A. A., Turner T. J., et al., 1995, ApJ, 438, 672

Magdziarz P., Zdziarski A. A., 1995, MNRAS, 273, 837

McNaron-Brown, K., et al., 1997, in preparation

Nandra K., George I. M., Mushotzky R. F., Turner T. J., Yaqoob Y., 1996, ApJ, in press

Nandra K., Pounds K., 1994, MNRAS, 268, 405

Nowak M. A., 1995, PASP, 718, 1207

Phlips B. F., Jung G. V., Leising M. D., et al., 1996, ApJ, 465, 907

Pounds K. A., Nandra K., Stewart G. C., George I. M., Fabian A. C., 1990, Nature, 344, 132

Poutanen J., Svensson R., 1996, ApJ, in press (PS96)

Poutanen J., Svensson R., Stern B., 1997, in: Winkler C., Courvousier T., Durouchoux P. (eds.) ESA SP-382, The Transparent Universe, in press

Stern B. E., Poutanen J., Svensson R., Sikora M., 1995, ApJ, 449, L13

Sunyaev R. A., Titarchuk L. G., 1980, A&A, 86, 121

Svensson R., 1984, MNRAS, 209, 175

Svensson R., 1987, MNRAS, 227, 403

Svensson R., 1996, A&AS, 120, in press

Tanaka Y., Inoue H., Holt S. S., 1994, PASJ, 46, L37

Tanaka Y., et al., 1995, Nature, 375, 659

Ueda Y., Ebisawa K., Done C., 1994, PASJ, 46, 107

Walter R., Fink H. H., 1993, A&A, 274, 105

White T. R., Lightman A. P., Zdziarski A. A., 1988, ApJ, 331, 939

Winkler C., 1994, ApJS, 92, 327

Zdziarski A. A., Fabian A. C., Nandra K., Celotti A., Rees M. J., Done C., Coppi P. S., Madejski G. M., 1994, MNRAS, 269, L55

Zdziarski A. A., Gierliński M., Gondek D., Magdziarz P., 1996, A&AS, 120, in press

Zdziarski A. A., Johnson W. N., Done C., Smith D., McNaron-Brown K., 1995, ApJ, 438, L63

Zdziarski A. A., Johnson W. N., Magdziarz P., 1996, MNRAS, 283, 193 (ZJM96)

Zdziarski A. A., Lightman A. P., Maciołek-Niedźwiecki A., 1993, ApJ, 414, L93